

## Resonant inelastic scattering of two x-ray photons by a many-electron atom

Alexey N. Hopersky, Alexey M. Nadolinsky, and Sergey A. Novikov\*  
 Chair of Mathematics, Rostov State Transport University, Rostov-on-Don 344038, Russia

 (Received 25 September 2018; published 20 December 2018)

A nonrelativistic variant of the quantum theory for the resonant inelastic-scattering process of two x-ray photons in the deep  $1s$ -shell ionization threshold energy region of a free many-electron atom is established. A quantitative estimate for the magnitude of the observed differential cross section is given.

DOI: [10.1103/PhysRevA.98.063424](https://doi.org/10.1103/PhysRevA.98.063424)

### I. INTRODUCTION

An x-ray free-electron laser (XFEL) realizes the possibility of investigating the fundamental processes of the nonlinear interaction of soft- and hard-x-ray radiation with a many-electron system [1]. To such processes, in particular, belongs the resonant inelastic scattering of two photons by an atom. This terminology is retained here due to its analogy to the process (Landsberg–Mandelstam, Raman, Compton) of scattering of a single photon by an atom [2], molecule [3], or solid matter [4]. Resonant inelastic scattering of two photons of hard XFEL radiation by matter in a condensed phase has recently been studied experimentally for the metallic films of germanium (Ge, nuclear charge  $Z = 32$ , energy of the absorbed XFEL photon is  $\hbar\omega \cong 5.6$  keV) [5], zirconium (Zr,  $Z = 40$ ,  $\hbar\omega \cong 9$  keV) [6], and copper (Cu,  $Z = 29$ ,  $\hbar\omega \cong 8.8$  keV,  $4.5$  keV) [7]. Such experiments prompt the task of constructing a theory for the process. In this paper, we construct the nonrelativistic variant of the quantum theory of resonant inelastic scattering of two x-ray photons in the deep  $1s$ -shell ionization threshold energy region of a free many-electron atom. The main result of the theory—prediction of the resonant  $K_{\alpha,\beta}$ -emission structure of the scattering spectrum—is consistent with the experimental results [5–7]. For the subject of the study, we take the atom of zinc (Zn,  $Z = 30$ , the configuration and term of the ground state are  $[0] = 1s^2 2s^2 2p^6 3s^2 3p^6 3d^{10} 4s^2 [^1S_0]$ ). This choice is dictated by the spherical symmetry of the ground state of Zn, as well as by the availability of the gaseous phase of Zn [8,9] for conducting high-precision XFEL experiments. We also note that the information about photon-scattering spectra of atomic Zn may be useful, for example, during the analysis of the structure and composition of thin films of matter [10], and the study of the prevalence of heavy metals in stellar atmospheres [11].

### II. THEORY

In the third order (over the  $\alpha$  fine structure constant) of the nonrelativistic quantum perturbation theory the process of resonant inelastic scattering of two photons in the  $1s$ -shell ionization threshold energy region of the Zn atom takes place

over two interfering (for a fixed value of orbital quantum number of the excited single electron state,  $l$ ) channels:

$$\omega + \omega + [0] \rightarrow \left\{ \begin{array}{l} D_{0,2} \\ Q_1 \rightarrow D_{0,2} \end{array} \right\} \rightarrow Y_{0,2} + \omega_C. \quad (1)$$

In Eq. (1) in the  $LS$ -coupling approximation the selection rules determine the initial  $|0\rangle = [0] \otimes (a_\omega^+)^2 |0_f\rangle$ , intermediate  $D_l = X_l \otimes |0_f\rangle$ ,  $X_l = 1sxl [^1S_0(l=0), ^1P_1(l=1), ^1D_2(l=2)]$ ,  $Q_1 = X_1 \otimes (a_\omega^+) |0_f\rangle$ , and final  $Y_C = Y_l \otimes (a_C^+) |0_f\rangle$ ,  $Y_l = np^5 \varepsilon l [^1P_1(l=0, 2)]$  scattering states, where  $xl > F$  is the Fermi level (set of atomic valence shell quantum numbers),  $\omega$  ( $\omega_C$ ) is the energy of the incident (scattered) photon,  $a_\omega^+$  ( $a_C^+$ ) is the creation operator for the incident (scattered) photon, and  $|0_f\rangle$  is the wave function of photon vacuum of quantum electrodynamics [12]. Here and thereafter, we assume the atomic system of units ( $m_e = e = \hbar = 1$ ), and the filled shells of the atomic configuration are not shown. The transition  $|0\rangle \rightarrow D_l$  occurs over the contact interaction operator:

$$\hat{C} = \frac{1}{2c^2} \sum_{n=1}^N (\hat{A}_n \cdot \hat{A}_n), \quad (2)$$

where  $c$  is the speed of light in vacuum,  $\hat{A}_n$  is the electromagnetic field operator in the second quantization picture at time  $t = 0$ , and  $N$  is the number of electron in the atom. Transitions  $|0\rangle \rightarrow Q_1 \rightarrow D_l \rightarrow Y_l$  occur via the operator of radiative absorption (emission):

$$\hat{R} = -\frac{1}{c} \sum_{n=1}^N (\hat{p}_n \cdot \hat{A}_n), \quad (3)$$

where  $\hat{p}_n$  is the momentum operator of the  $n$ th atomic electron. Corresponding to the channels (1), the scattering probability amplitudes take the following form:

$$A_l = \int_0^\infty dx \frac{\langle 0 | \hat{C} | D_l \rangle \langle D_l | \hat{R} | Y_C \rangle}{\Delta_x + i\gamma_{1s}}, \quad (4)$$

$$B_l = \int_0^\infty \int_0^\infty dx dy \frac{\langle 0 | \hat{R} | Q_1 \rangle \langle Q_1 | \hat{R} | D_l \rangle \langle D_l | \hat{R} | Y_C \rangle}{(\Delta_x + \omega + i\gamma_{1s})(\Delta_y + i\gamma_{1s})}, \quad (5)$$

where  $\Delta_x = x - 2\omega + I_{1s}$ ,  $I_{1s}$  is the  $1s$ -shell ionization energy threshold,  $\gamma_{1s} = \Gamma_{1s}/2$ , and  $\Gamma_{1s}$  is the natural linewidth of the  $1s$ -vacancy decay. The imaginary parts  $i\gamma_{1s}$  of the

\*sanovikov@gmail.com

energy denominators remove the singularity of the integrand functions of the improper integrals (4) and (5). In Eqs. (4) and (5), the matrix elements are calculated through the methods of the photon creation (annihilation) operator algebra and the theory of irreducible tensor operators representations (see Appendix A). During the construction of the differential cross section of the process, we carry out the summation over the projections of the full momentum of the final  $Y_l$  states of the atom ( $M = -1, 0, +1$ ), and the averaging over the projections over the initial atomic state [ $M = 0, (2J + 1)^{-1} = 1$ ]. During the construction of the single-electron matrix element of the free-free radiative transition and overlap integrals for the continuous energy spectrum wave functions, the plane-wave approximation is taken  $|x\rangle \approx \sin(r\sqrt{2x})$ . In this case, taking into account the equality [13] [ $\Gamma(\alpha)$  is the Euler gamma function]:

$$\int_0^\infty x^{\alpha-1} e^{-\rho x} \cos(bx) dx = \frac{\Gamma(\alpha)}{(b^2 + \rho^2)^{\alpha/2}} \cos \left\{ \alpha \arctan \left( \frac{b}{\rho} \right) \right\}, \quad (6)$$

$\text{Re } \alpha > 0, \quad \text{Re } \rho > |\text{Im } b|.$

Then, for  $\text{Im } b = 0$  and  $\rho \rightarrow 0$  we obtain ( $\delta$  is the Dirac  $\delta$ -function)

$$(x - y)\langle x|r|y\rangle \cong 2ix\delta(x - y), \quad \alpha = 2, \quad (7)$$

$$\langle x|\varepsilon\rangle \cong \delta(x - \varepsilon), \quad \alpha = 1. \quad (8)$$

For small energies of the  $l$  electrons of the continuous spectrum, the  $l$ -symmetry-dependent effect of delocalization of radial parts of wave functions of electrons in the deep  $1s$ -vacancy field is significant. As a result, analytical structures of integrals (7) and (8) outside of the plane-wave approximation are made more complex (see Appendix A). Going beyond the plane-wave approximation framework is a subject of future investigations.

The physical interpretation for the scattering probability amplitudes in the Feynman diagram representation is shown in Figs. 1(a) (amplitude  $A_l$ ) and 1(b) (amplitude  $B_l$ ). The remaining wide set of the scattering amplitudes is not taken into account due to the assumed Tamm–Dancoff approximation [14,15]. In this approximation, for a fixed set of  $\hat{C}$  and  $\hat{R}$  operators in the Feynman diagram representation only the amplitudes whose dissections contain the minimal number of photons, electrons, and vacancies, are taken into account. The Tamm–Dancoff approximation is widely used in atomic physics [16], yet it still does not have an analytical justification (see, for example, Silin *et al.* [14]). In particular, the question remains about the gauge invariance of this approximation, and as a result, about such invariance of the theory developed in this work.

Note that the  $|0\rangle \rightarrow D_2$  transition is suppressed relative to the  $|0\rangle \rightarrow D_0$  transition:  $\langle 1s|j_2|\varepsilon d\rangle \ll \langle 1s|j_0|\varepsilon s\rangle$ . For the  $\hat{R}$  operator, let us make the dipole approximation [ $\exp(\pm i\vec{k} \cdot \vec{r}_n) \cong 1$ , where  $\vec{k}$  is the wave vector of the incident (scattered) photon, and  $\vec{r}_n$  is the radius-vector of the  $n$ th atomic electron], since for the Zn atom with  $\omega \cong 5$  keV ( $\lambda \cong 2.48$  Å) and average  $1s$ -shell radius of  $\langle r_{1s} \rangle = 0.027$  Å, the inequality

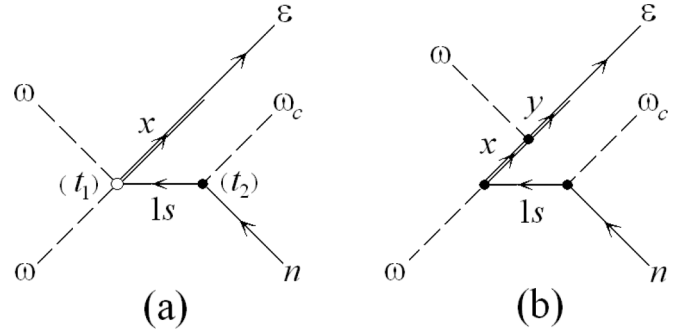


FIG. 1. Partial probability amplitudes for the resonant inelastic scattering of two XFEL photons by the Zn atom in the Feynman diagram representation. Right arrow is the electron [ $\varepsilon \equiv \varepsilon(s, d)$ ], left arrow is the vacancy ( $n \equiv np_j$ ). Light (dark) circle shows interaction vertex over the contact (radiative) transition operator. Double line shows the state obtained in the Hartree–Fock field of the  $1s$  vacancy.  $\omega$  ( $\omega_c$ ) is the incident (scattered) photon. Time direction for the process is  $t_1 < t_2$ .

$\lambda/\langle r_{1s} \rangle \cong 92 \gg 1$  holds. Let us also take into account the applicability of Fermi’s golden rule [17]:

$$\hbar E_0^{-1} \ll \tau_{\text{XFEL}} \ll \tau_0, \quad (9)$$

for the Zn atom (the energy and lifetime of the ground state are  $E_0 \cong 48.807$  keV and  $\tau_0 \cong \infty$ , respectively) is satisfied:  $\tau_{\text{XFEL}} \gg 10^{-5}$  fs,  $1$  fs =  $10^{-15}$  s. Here, the duration of the XFEL pulse, for example, for the conducted experiments is  $\tau_{\text{XFEL}} \cong 2.5$  [5],  $10$  [6], and  $30$  [7] fs. Then, taking into account the ratio of the statistical weights for the  $np_j$  vacancies of the final states [branching coefficient  $(l + 1)/l = 2$ ], and summing the scattering probabilities over the  $s$  and  $d$  channels (1), we obtain for the full scattering differential cross section:

$$\frac{d\sigma_\perp}{d\omega_c} \equiv \sigma_\perp^{(1)} = \eta\omega_c \sum_j \mu_j \int_0^\infty \frac{\psi(\varepsilon)}{\varepsilon_j} d\varepsilon, \quad (10)$$

$$\mu_j = (2j + 1)\gamma_j \left( \frac{\omega_j R_j}{\omega} \right)^2, \quad (11)$$

$$\varepsilon_j = (\Delta_\varepsilon^2 + \gamma_{1s}^2) [(\Delta_\varepsilon - \Delta_j)^2 + \gamma_j^2], \quad (12)$$

$$\psi(\varepsilon) = \gamma_{1s} \zeta \left[ \frac{a_1 \zeta - a_2 S}{(\Delta_\varepsilon + \omega)^2 + \gamma_{1s}^2} \right] + a_3 S^2. \quad (13)$$

Here, the following quantities are defined:  $\eta/r_0^2 = (1/6) \times 10^{-36}$ ,  $r_0$  is the classical electron radius,  $\gamma_j = \Gamma_j/2$ ,  $\Gamma_j$  is the natural linewidth of the  $np_j$  vacancy decay, the energy of the resonance for  $K_{\alpha,\beta}$  emission ( $K_{\alpha_1,\beta_1}$ ,  $j = 3/2$ ;  $K_{\alpha_2,\beta_2}$ ,  $j = 1/2$ ) is  $\omega_j = I_{1s} - I_j$ , where  $I_j$  is the ionization threshold energy for the  $np_j$  shell,  $R_j$  is the radial part of the radiative  $1s \rightarrow np_j$  transition amplitude,  $\Delta_j = \omega_j - \omega_c$ ,  $\zeta = \varepsilon(\varepsilon + I_{1s})M$ ,  $M$  is the radial part of the radiative  $1s \rightarrow \varepsilon p$  transition amplitude,  $S$  is the radial part of the contact  $|0\rangle \rightarrow X_0$  transition,  $a_1 = 1.112/\gamma_{1s}$ ,  $a_2 = 28.86$  and  $a_3 = 208.23$ . The quantity  $\gamma_j$  in Eq. (10) appears because of the substitution of the Dirac  $\delta$  function  $\delta(2\omega - \omega_c - I_j - \varepsilon)$  in Fermi’s golden rule for a Lorentzian  $L_j = (\gamma_j/\pi)[(2\omega - \omega_c - I_j - \varepsilon)^2 + \gamma_j^2]^{-1}$  with the subsequent integration (the  $\varepsilon l$  electron is not

registered in the experiment) over  $\varepsilon \in [0; \infty)$ . The symbol “ $\perp$ ” in Eq. (10) corresponds to the choice for the scheme of the assumed XFEL experiment: the wave vectors (polarization vectors) of the linearly polarized incident and scattered photons belong (perpendicular,  $\perp$ ) to the scattering plane. We note that, in light of the assumed dipole approximation as well as the Tamm–Dancoff approximation, the expression (10) does not depend on the  $\omega_C$ -photon-scattering angle (isotropic scattering):

$$\frac{d^3\sigma_{\perp}}{d\omega_C d\Omega_C d\varepsilon} \rightarrow \frac{1}{4\pi} \sigma_{\perp}^{(1)}, \quad (14)$$

where  $\Omega_C$  is the solid angle of flight of the scattered photon. However, outside of the Tamm–Dancoff approximation, this work’s methods predict (Hopersky and Nadolinsky [16]) scattering-angle-dependent x-ray emission of the quadrupole type (in the sense that  $\Delta l = 0, 2$  during the transition  $1s_{1/2} \rightarrow nl_j + \omega_C$ ) through operator  $\hat{C}$ . Indeed, within the  $LS$ -coupling approximation the selection rules allow, for example, the following process:

$$\omega + \omega + [0] \rightarrow Q_1 \rightarrow nl_j^{4l+1} \varepsilon p + \omega_C,$$

where  $l_j = s_{1/2}, d_{3/2,5/2}$ . Probability amplitudes of this process do not interfere with the probability amplitudes of process (1) and contain the matrix element of the single-electron contact  $j_l$  operator of the emissive transition  $\langle 1s | j_l(qr) | nl_j \rangle$ . Here,

$$q = (\omega/c) \sqrt{1 + \chi^2 - 2\chi \cos \theta_S},$$

$\chi = \omega_C/\omega$ ,  $\theta_S$  are the scattering angles (the angles between the wave vectors of the incident and scattered photons) and the resonant energy of the scattered photon depends [in contrast to  $\omega_C$  from Eq. (10)] on the XFEL photon energy:  $\omega_C^{\text{res}} \cong \omega + I_{1s} - I(nl_j)$ , where  $I(nl_j)$  is the energy of the ionization threshold of the  $nl_j$  shell,  $\omega \geq I_{1s}$ . Here, (i) the  $1s_{1/2} \rightarrow 3d_{3/2,5/2} + \omega_C$  transition does not correspond to the well-known (Blochin [18])  $K_{\beta_5}^{II,I}$  resonances of the heavy-atom x-ray emission spectrum, and (ii) the  $1s_{1/2} \rightarrow ns_{1/2} + \omega_C$  transition ( $n \geq 1$ ) is allowed, forbidden for the quadrupole part of operator  $\hat{R}$  by the vacancy quantum number selection rules ( $l_1 + l_2 \geq 2$ ,  $j_1 + j_2 \geq 2$ ) [17].

Also note that the numerical integration result in Eq. (10) reproduces the well-known analytical result of the Weisskopf–Wigner theory [18]:

$$\int_{-\infty}^{+\infty} \varepsilon_j^{-1} d\varepsilon = \left( \frac{\pi \gamma}{\gamma_{1s} \gamma_j} \right) (\Delta_j^2 + \gamma^2)^{-1}. \quad (15)$$

In Eq. (15), the “observed” linewidth for the resonance of the  $K_{\alpha,\beta}$  emission is defined as a sum of the natural decay linewidths of the  $1s$  and  $np_j$  vacancies:  $\gamma = \gamma_{1s} + \gamma_j$ .

The appearance of the deep  $1s$ -vacancy in the shell of the many-electron atom is accompanied by the effect of monopole (without changing the symmetry of the atomic state) rearrangement of the radial parts of the single-electron state wave functions. We include this effect via the theory of nonorthogonal orbitals [19]. In case of the Zn atom,

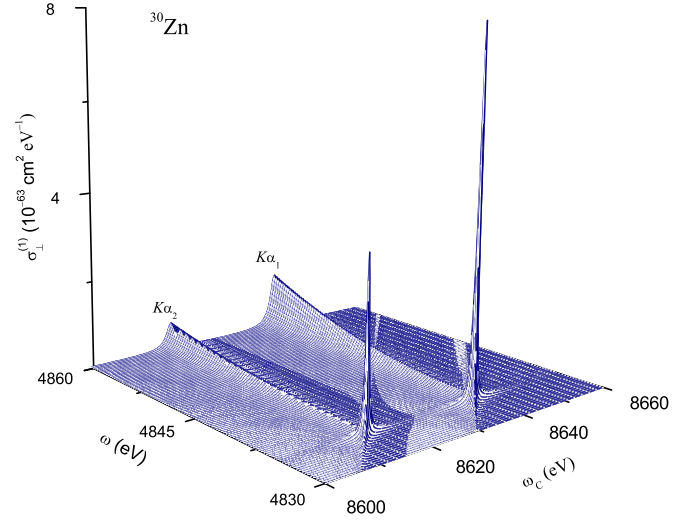


FIG. 2. Differential cross section for the resonant inelastic scattering of two XFEL photons by the Zn atom in the  $K_{\alpha_{1,2}}$ -emission region.  $2\omega \cong I_{1s}$ ,  $I_{1s} = 9671.05$  eV.  $\omega(\omega_C)$  is the energy of the incident (scattered) photon. Spectral characteristics of the discrete spectrum resonances are given in Table I.

we obtain

$$M = \langle 1s_0 | r | \varepsilon p \rangle_C, \quad (16)$$

$$S = \langle 1s_0 | j_0 | \varepsilon s \rangle_C. \quad (17)$$

Here are defined the correlation function

$$|\varepsilon l\rangle_C = N_{1s} \left( |\varepsilon l_+\rangle - \sum_{m \leq F} |ml_+\rangle \rho_l \right), \quad (18)$$

$$N_{1s} = \langle 1s_0 | 1s_+ \rangle \prod_{n \leq F} \langle nl_0 | nl_+ \rangle^{4l+2}, \quad nl \neq 1s, \quad (19)$$

$$\rho_l = \langle ml_0 | ml_+ \rangle^{-1} \langle ml_0 | \varepsilon l_+ \rangle, \quad (20)$$

and the spherical Bessel function  $j_0 = (qr)^{-1} \sin(qr)$ ,  $q = 2\omega/c$ . The radial parts of the wave functions of the single-electron  $l_0(l_+)$  states are obtained by solving the integro-differential equations of the self-consistent Hartree–Fock field for the  $[0] ([1s_+\varepsilon(s, p)_+])$  atomic configuration. In Eq. (16) the single-electron operator for the radiative transition is left in the  $r$  form for the radius to account for the inter- and intrashell correlations (Amusia [19]) during the excitation (ionization) of the inner  $1s$  shell of the many-electron atom does not (within  $\sim 1\%$ ) change the results of the single-configuration Hartree–Fock approximation (Hopersky and Yavna [19]).

### III. RESULTS AND DISCUSSION

The calculation results for the differential cross section (10) for the Zn atom in the XFEL photon energy region of  $2\omega \cong I_{1s}$  are shown in Figs. 2–5 and in Table I. The calculation parameters are determined as follows:  $I_{1s} = 9671.05$  eV (our relativistic calculation),  $\Gamma_{1s} = 1.67$  eV [20],

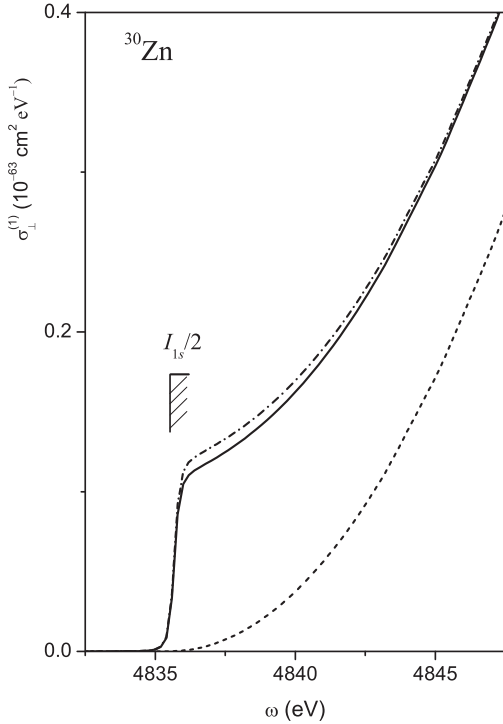


FIG. 3. Same as in Fig. 2, but for a fixed value of  $\omega_C(K_{\alpha_1}) = 8638.99$  eV. Solid curve:  $\hat{C}$  and  $\hat{R}$  operators and the monopole rearrangement effect (MRE) are taken into account. Dashed curve:  $\hat{R}$  operator and MRE are taken into account. Dashed-dot curve:  $\hat{C}$  and  $\hat{R}$  operators but not MRE are taken into account.

$\Gamma_j = 0.72$  eV ( $j = 1/2$ ),  $0.65$  eV ( $j = 3/2$ ) [20],  $\omega_j = 8615.89$  eV ( $j = 1/2$ ),  $8638.99$  eV ( $j = 3/2$ ) [21] for the  $K_{\alpha}$ -emission resonances, and  $\Gamma_j = 1.70$  eV ( $j = 1/2$ ),  $2.00$  eV ( $j = 3/2$ ) [22],  $\omega_j = 9572.35$  eV ( $j = 1/2$ ),  $9574.95$  eV ( $j = 3/2$ ) for the  $K_{\beta}$ -emission resonances. The last two values are obtained from the equality  $\omega_j = I_{1s} - I_j$ , where  $I_{3/2} = 96.10$  eV and  $I_{1/2} = 98.70$  eV are taken from Ref. [23]. We note that recently measured [24] values for the  $K_{\beta_{1,3}}$ -emission resonance energies for Zn in the metallic phase,  $\omega_j = 9572.234$  eV ( $j = 3/2$ ),  $9569.322$  eV ( $j = 1/2$ ), deviate only by about 0.03% from the values assumed by us during the differential-cross-section calculation (10).

In Figs. 2 and 5 and in Table I the subthreshold ( $2\omega < I_{1s}$ ) discrete structure of the scattering spectrum is represented only by the most intense channel (1):  $1s4p(^1P_1) \rightarrow 1s4d(^1D_2) \rightarrow (2p, 3p)^54d(^1P_1)$ . Inclusion of a wide series of other scattering channels in this region of XFEL photon energies is a subject of future investigation. The “ribbed” structures of the resonances in Figs. 2 and 5 are due to

$$\sigma_{\perp}^{(1)} \sim [(2\omega - I_{1s4d})^2 + \gamma_{1s}^2]^{-1} [(2\omega - \Lambda_j - \omega_C)^2 + \gamma_j^2]^{-1}, \quad (21)$$

where  $I_{1s4d} = E(1s4d) - E(0)$ ,  $\Lambda_j = E(np_j^54d) - E(0)$ , and  $E$  are the total Hartree–Fock energies of the atomic states. As a result, the differential cross section in the plane of variables  $\omega$  and  $\omega_C$  becomes maximal on the straight line

$$2\omega = \omega_C \tan(\varphi) + \Lambda_j, \quad \varphi = \pi/4. \quad (22)$$

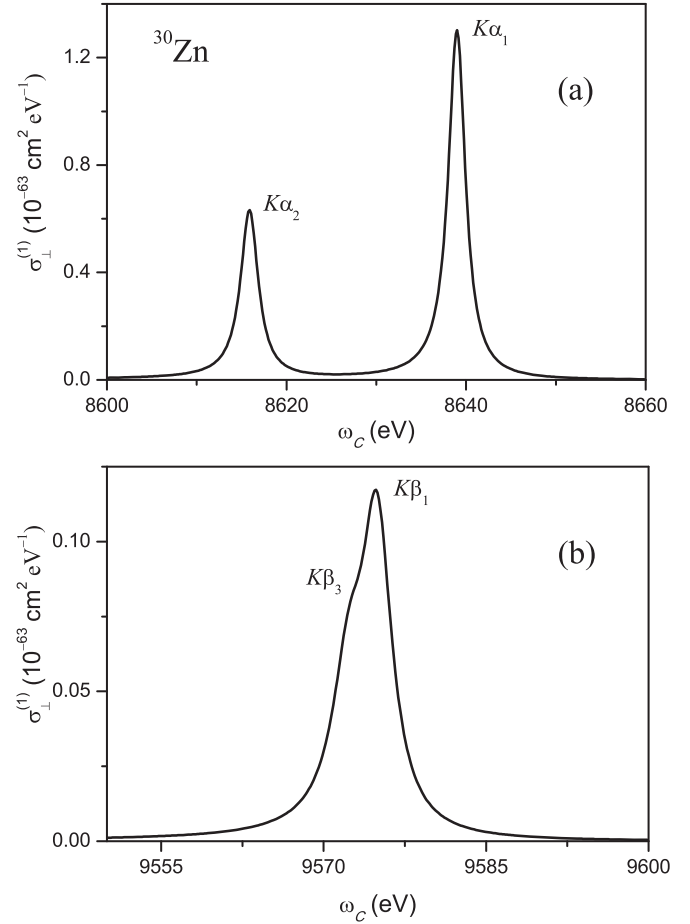


FIG. 4. Weisskopf–Wigner effect during the resonant inelastic scattering of two XFEL photons by the Zn atom in the region of (a)  $K_{\alpha_{1,2}}$  and (b)  $K_{\beta_{1,3}}$  emission.  $\omega = 4860$  eV,  $\delta_{SO}(K_{\alpha}) = 23.1$  eV,  $\delta_{SO}(K_{\beta}) = 2.6$  eV.  $\omega$  ( $\omega_C$ ) is the energy of the incident (scattered) photon.

Here, the maximum of the local resonance is determined by the first factor in Eq. (21). In particular, in Table I the values of the main maxima of  $\sigma_{\perp}^{(1)}$  with  $2\omega = I_{1s4d}$  are presented.

In contrast with the case of resonant inelastic scattering of a single photon by a many-electron atom [25–30], the braking absorption of the second XFEL photon by the virtual  $xp$  electron of the continuous spectrum [Fig. 1(b)] determines the appearance of the  $\zeta$  function in Eq. (13). As a result, the behavior of the scattering cross section changes qualitatively in the near post-threshold ( $2\omega \geq I_{1s}$ ) XFEL photon energy (Fig. 3). Indeed, neglecting the contribution of the contact scattering channel [Fig. 1(a)], we have  $\sigma_{\perp}^{(1)} \sim (1 - I_{1s}/2\omega)^2 M^2$  and  $\sigma_{\perp}^{(1)} \rightarrow 0$  with  $\omega \rightarrow I_{1s}/2$ . In the far post-threshold scattering region the behavior of  $\sigma_{\perp}^{(1)}$  is determined by the behavior of the amplitude  $M$  from (16):  $\sigma_{\perp}^{(1)} \sim M^2 \rightarrow 0$  when  $\omega \rightarrow \infty$ . Taking into account the scattering channel over the  $\hat{C}$  operator recovers  $\sigma_{\perp}^{(1)}$  to a nonzero value. Thus, the principally important role of the  $\hat{C}$  operator in process (1) is established in the  $1s$ -shell many-electron atom ionization threshold energy region. As  $\omega$  increases, the role of the  $\hat{C}$  operator decreases significantly, and when  $2\omega \gg I_{1s}$ , the cross

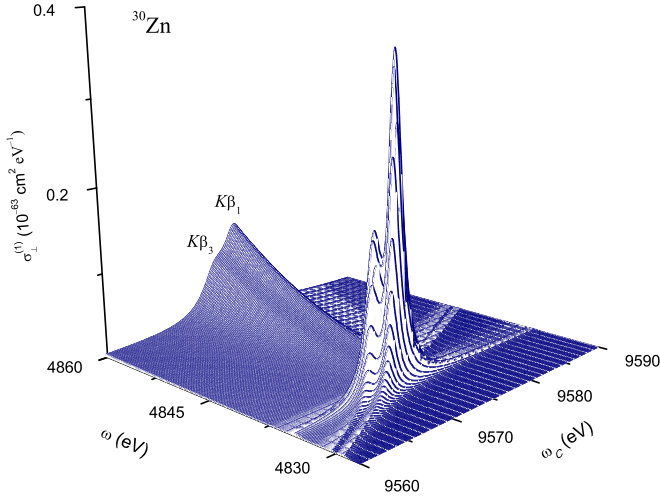


FIG. 5. Same as in Fig. 2, but for the region of  $K_{\beta_{1,3}}$  emission.

section of process (1) is practically determined by just the  $\hat{R}$  operator. The effect of monopole rearrangement of electron shells for the Zn atom only insignificantly (Fig. 3) changes the calculation result in the “frozen” core atomic ground-state approximation. Indeed, the Hartree–Fock field of the arising deep  $1s$  vacancy for the virtual electrons of the continuous spectrum is strongly screened by the ground-state shells of the heavy many-electron atom.

The results in Fig. 4(a) demonstrate the Weisskopf–Wigner effect [18]:  $\Gamma(K_{\alpha_1}) = \Gamma_{1s} + \Gamma_{3/2} = 2.32$  eV,  $\Gamma(K_{\alpha_2}) = \Gamma_{1s} + \Gamma_{1/2} = 2.39$  eV. The small ( $\sim 3\%$ ) difference from the values in Fig. 4(a) is due to the effect of “overlying” of the Lorentzian profiles of  $K_{\alpha_1}$ - and  $K_{\alpha_2}$ -emission resonances. For the  $K_{\beta_1}$ - and  $K_{\beta_3}$ -emission resonances [Fig. 4(b)] the Weisskopf–Wigner effect is spectrally “washed out” by the fact that  $\Gamma_j(3p) > \Gamma_j(2p)$  and  $\delta_{SO}(K_{\beta}) = 2.6$  eV  $<$   $\delta_{SO}(K_{\alpha}) = 23.1$  eV, where  $\delta_{SO}$  is the spin-orbit splitting constant of the  $np_j$  shell. The absence of analytical solutions to the Hartree–Fock equation leaves only the possibility of numerical integration in Eq. (10) (Appendix B). The fact that it reproduces the Weisskopf–Wigner effect makes it even more incredible, because both the lower integration limits [ $\varepsilon = -\infty$  in Eq. (15) and  $\varepsilon = 0$  in Eq. (10)], and the integrands [ $\psi = 1$  in Eq. (15) and  $\psi \neq 1$  in Eq. (10)] are different. From the mathematical standpoint an analytical proof of this fact is

TABLE I. Spectral characteristics for the leading  $1s \rightarrow 4p \rightarrow 4d$  resonances of the discrete part of the spectrum for resonant inelastic scattering of two XFEL photons by the atom of Zn in the  $K_{\alpha,\beta}$ -emission region.  $2\omega = I_{1s4d} = 9669.51$  eV,  $I_{1s} = 9671.05$  eV.  $\omega(\omega_c)$  is the energy of the incident (scattered) photon,  $\sigma_{\perp}^{(1)}$  is the differential scattering cross section.

$K_{\alpha,\beta}$	$\omega_c$ (eV)	$\sigma_{\perp}^{(1)} \times 10^{63}$ (cm <sup>2</sup> eV <sup>-1</sup> )
$K_{\alpha_1}$	8638.862	8.203
$K_{\alpha_2}$	8615.938	3.676
$K_{\beta_1}$	9571.382	0.369
$K_{\beta_3}$	9568.883	0.184

doubtlessly of great interest and deserves an independent investigation.

In works [21,24] the authors did not measure the differential cross section (10). Therefore, the comparison of the results of our theory with experiment [21,24] measuring the x-ray  $K_{\alpha,\beta}$ -emission spectra of the Zn atom in the metallic phase carries a vicarious character. Nevertheless, the forms and relative magnitudes for the differential scattering cross sections in Figs. 4(a) and 4(b) practically reproduce the forms and relative magnitudes of the emission spectra in Fig. 2 ( $K_{\alpha_{1,2}}$ ) of Ref. [21] and Fig. 8 ( $K_{\beta_{1,3}}$ ) of Ref. [24].

Finally, let us provide a qualitative estimate for the magnitude of the “observed” differential scattering cross section in the presumed XFEL experiment. Due to the theorem about the sum of probabilities for mutually exclusive events [31]; for example, for  $\omega = 4860$  eV and  $\omega_c = 8638.99$  eV ( $K_{\alpha_1}$ -emission resonance energy) with the obtained [1] average laser radiation brightness level of  $N = 10^{12}$  (number of photons in the XFEL pulse) we obtain  $C_N^2 \sigma_{\perp}^{(1)} \cong 6.5 \times 10^{-22}$  (Mb eV<sup>-1</sup>), where  $C_N^2$  is the binomial coefficient. With the expected [32] average brightness level of  $N = 10^{23}$  we obtain a value quite accessible to experimental measurement:  $C_N^2 \sigma_{\perp}^{(1)} \cong 6.5$  (Mb eV<sup>-1</sup>).

#### IV. CONCLUSION

Let us formulate the main results of this work. A nonrelativistic variant of the theory for the process of resonant inelastic scattering of two x-ray photons in the deep  $1s$ -shell ionization threshold of a free many-electron atom is constructed within the framework of quantum-mechanical perturbation theory. The theory is free from the so-called “infrared divergence” ( $\omega_c \rightarrow 0 \Rightarrow \sigma \rightarrow \infty$ ), which is inherent in the theory of resonant Compton scattering of one photon by an atom [2]. Indeed, according to Eq. (10) we have  $\omega_c \rightarrow 0 \Rightarrow \sigma \rightarrow 0$ . The atom Zn is considered. The theory predicts a pronounced  $K_{\alpha,\beta}$ -emission structure of the scattering spectrum. The methods of the current work also predict the appearance of emission structures of a new physical type—structures of quadrupole x-ray emission via the contact-interaction operator—in the spectrum of resonant inelastic scattering of two x-ray photons by a many-electron atom. Exploring this prediction in detail is a subject of future investigation. We establish the principally important role for the contact-interaction operator in the near post-threshold scattering region. Due to this fact, the process investigated here drastically differs from the process of resonant inelastic scattering of a single photon by a many-electron atom. As the XFEL photon energy departs further away from the  $1s$ -shell ionization threshold, the role of contact scattering decreases and the differential cross section of the process is determined practically by just the radiative transition operator. It is also found that, in the energy region for the creation of the final scattering states of the continuous spectrum, the theory reproduces the Weisskopf–Wigner effect for the “observable”  $K_{\alpha,\beta}$ -emission resonance linewidths. Further development of the theory concerns, first of all, going beyond the framework of the Tamm–Dancoff approximation, and taking into account (i) the wide series of scattering channels in the subthreshold XFEL photon energy region, (ii) the effects of configurational

mixing in the scattering channels, and (iii) the completeness of the set of single-electron states of the discrete spectrum of the virtual (intermediate) and final scattering states (Hopersky and Nadolinsky [19]). Of interest is also the generalization of the theory; in particular to multiply charged atomic ions of isoelectronic sequences with intense discrete structures of the photoabsorption spectra. We also note that in the close near-threshold XFEL photon energy region, for example, for the  $K_{\beta_1}$ -emission discrete resonance energy (Table 1), the equality  $\omega_C(K_{\beta_1}) \cong 2\omega$  is practically satisfied (to within  $\sim 1\%$ ). Therefore, in this laser radiation energy region, process (1) becomes the practical (but not the theoretical) analog of the “merging” effect for XFEL photons in the field of an atom [33] and an atomic ion [34]. The estimate for the absolute value of the differential scattering cross section points to the possibility of an experimental discovery of the predicted  $K_{\alpha,\beta}$ -emission structures with the XFEL-radiation brightness level expected in the near future.

### APPENDIX A

As an example, let us carry out the construction of the matrix element  $\langle D_2 | \hat{R} | Y_C \rangle$ .

Consider the second-quantization representation:

$$\hat{A}_n = \sum_{\vec{k}} \sum_{\rho=1,2} \vec{e}_{\vec{k}\rho} (a_{\vec{k}\rho}^+ + a_{\vec{k}\rho}^-), \quad (\text{A1})$$

$$a_{\vec{k}\rho}^+ |n_{\vec{k}\rho}\rangle = \sqrt{\theta(n_{\vec{k}\rho} + 1)} |n_{\vec{k}\rho} + 1\rangle, \quad \theta = \frac{2\pi c^2}{V\omega}, \quad (\text{A2})$$

$$a_{\vec{k}\rho}^- |n_{\vec{k}\rho}\rangle = \sqrt{\theta n_{\vec{k}\rho}} |n_{\vec{k}\rho} - 1\rangle, \quad (\text{A3})$$

$$a_{\vec{k}\rho}^- a_{\vec{k}\rho}^+ - a_{\vec{k}\rho}^+ a_{\vec{k}\rho}^- = \theta. \quad (\text{A4})$$

Here, for operator  $\hat{A}_n$  we take the dipole approximation [ $\exp(\pm i\vec{k} \cdot \vec{r}_n) \cong 1$ ],  $\vec{e}_{\vec{k}\rho}(\vec{k})$  is the polarization vector (wave vector) of the photon,  $\omega$  is the photon angular frequency,  $n_{\vec{k}\rho}$  is the photon occupation number, and  $V$  is the electromagnetic-field quantization volume [we used  $V \text{ (cm}^3\text{)} = c$  [35]]. Consider the relation between the forms of the radius and velocity for the radiative transition operator:

$$\langle \gamma | \hat{P} | \gamma' \rangle = i(E_{\gamma} - E_{\gamma'}) \langle \gamma | \hat{D} | \gamma' \rangle, \quad (\text{A5})$$

$$\hat{P} = \sum_{n=1}^N \hat{p}_n, \quad (\text{A6})$$

$$\hat{D} = \sum_{n=1}^N \vec{r}_n, \quad (\text{A7})$$

where  $E_{\gamma,\gamma'}$  are the energies of  $\gamma$  and  $\gamma'$  states of the atom. Let us define the operator

$$Q_p^{(1)} = \sum_{n=1}^N C_p^{(1)}(\vec{q}_n) r_n, \quad (\text{A8})$$

where  $C_p^{(1)}$  is the spherical function,  $r_n$  is the magnitude of vector  $\vec{r}_n$ , and  $\vec{q}_n$  is the unit vector in the direction of  $\vec{r}_n$ . Taking

into account (A8) we have in the structure of the  $\hat{R}$  operator:

$$(\vec{e}_C \cdot \hat{P}) \rightarrow (\vec{e}_C \cdot \hat{D}) = \sum_{p=-1}^{+1} (-1)^p C_{-p}^{(1)}(\vec{e}_C) Q_p^{(1)}, \quad (\text{A9})$$

where  $\vec{e}_C$  is the scattered photon polarization vector. Taking into account the Wigner–Eckart theorem:

$$\begin{aligned} & \langle X_2, M | Q_p^{(1)} | Y_2, \bar{M} \rangle \\ &= (-1)^{2-M} \begin{pmatrix} 2 & 1 & 1 \\ -M & p & \bar{M} \end{pmatrix} \langle X_2 || Q^{(1)} || Y_2 \rangle, \end{aligned} \quad (\text{A10})$$

where we define the Wigner  $3j$  symbol and  $M(\bar{M})$  is the projection of the total angular momentum  $J = 2$  ( $\bar{J} = 1$ ). Taking into account formulas (29.3) and (29.6) of Ref. [36] and the equalities for the  $6j$  and  $9j$  symbols ( $[x] \equiv 2x + 1$ ,  $\delta_{ab}$  is the Kronecker–Weierstrass symbol):

$$\begin{Bmatrix} a & b & 0 \\ d & c & f \end{Bmatrix} = (-1)^{a+d-f} \frac{\delta_{ab}\delta_{cd}}{\sqrt{[c, b]}}, \quad (\text{A11})$$

$$\begin{Bmatrix} f & b & d \\ 0 & e & e \\ f & a & c \end{Bmatrix} = (-1)^{b+c+e+f} \frac{1}{\sqrt{[e, f]}} \begin{Bmatrix} a & b & e \\ d & c & f \end{Bmatrix}, \quad (\text{A12})$$

for the reduced matrix element in Eq. (A10) for the case of the  $K_{\alpha}$  emission, we have:

$$\langle X_2 || Q^{(1)} || Y_2 \rangle = -2\sqrt{5} \langle 1s | r | 2p \rangle \delta(x - \varepsilon). \quad (\text{A13})$$

Finally, taking into account the structure of the  $\hat{R}$  operator as well as formulas (A1) through (A13), we have

$$\langle D_2 | \hat{R} | Y_C \rangle = i \left( \frac{40\pi}{V\omega_C} \right)^{1/2} \omega(K_{\alpha}) \langle 1s | r | 2p \rangle \delta(x - \varepsilon) \Phi_{M\bar{M}}, \quad (\text{A14})$$

$$\Phi_{M\bar{M}} = \sum_{p=-1}^{+1} (-1)^{p+M} C_{-p}^{(1)}(\vec{e}_C) \cdot \begin{pmatrix} 2 & 1 & 1 \\ -M & p & \bar{M} \end{pmatrix}, \quad (\text{A15})$$

where  $\omega(K_{\alpha}) = \omega_j$  for the  $2p_j$  shell.

Through the structure (A15), we carry out the summation over the  $M$  and  $\bar{M}$  projections when constructing the differential scattering cross section. During this, we take into account the theorem of summation of spherical functions,

$$\sum_M C_M^{(1)}(\vec{a}) C_M^{(1)*}(\vec{b}) = P_1(\cos \Psi), \quad (\text{A16})$$

and the condition of orthogonality of the Wigner  $3j$  symbols,

$$\sum_{jm} (2j+1) \begin{pmatrix} j_1 & j_2 & j \\ m_1 & m_2 & m \end{pmatrix} \begin{pmatrix} j_1 & j_2 & j \\ n_1 & n_2 & m \end{pmatrix} = \delta_{m_1 n_1} \delta_{m_2 n_2}. \quad (\text{A17})$$

In Eq. (A16) we define  $P_1$  as the spherical Legendre polynomial, and  $\Psi$  as the angle between vectors  $\vec{a}$  and  $\vec{b}$ .

During the construction of the  $\hat{C}$ -operator matrix elements beyond the dipole approximation for the Bessel  $j_t$  functions, the following mathematical results are taken into account:

(i) Decomposition of the exponent appearing in (2) into a double functional series (Rayleigh's formula) [37]:

$$\exp\{i(\vec{s} \cdot \vec{r}_n)\} = \sum_{t=0}^{\infty} i^t [t] j_t(sr_n) T_t, \quad (\text{A18})$$

$$T_t = \sum_{p=-t}^t (-1)^p C_{-p}^{(t)}(\vec{e}_s) C_p^{(t)}(\vec{q}_n), \quad (\text{A19})$$

where  $s$  is the magnitude of vector  $\vec{s}$ ,  $\vec{e}_s$  is the unit vector in the direction of  $\vec{s}$ .

(ii) The integral Plana–Poisson representation for the spherical Bessel function of the first kind of order  $t$  [38]:

$$j_t(x) = \frac{1}{t!} \left(\frac{x}{2}\right)^t \int_0^1 (1-z^2)^t \cos(xz) dz, \quad x \in [0; \infty). \quad (\text{A20})$$

(iii) The expression for the reduced matrix element,

$$(0 \| Q^{(t)} \| X_l) = \sqrt{2} \delta_{lt} \langle 1s | j_t | xl \rangle, \quad (\text{A21})$$

of the contact-interaction operator over the  $p$  multipolarity

$$Q_p^{(t)} = \sum_{n=1}^N C_p^{(t)}(\vec{q}_n) j_t(sr_n). \quad (\text{A22})$$

Beyond the plane-wave approximation for the continuous spectrum wave functions, the singular multiplicative factors, in particular, in the radiative transition probability amplitude (A14), are modified. The corresponding analytical expressions for the overlap integrals and probability amplitudes of the free-free radiative transitions are obtained in Ref. [39] (and references therein). In particular, in the single-configuration Hartree–Fock approximation, for the states obtained in different Hartree–Fock potentials, instead of Eq. (8) we have (Novikov and Hopersky [39])

$$\langle x | \varepsilon \rangle \rightarrow \cos(\varphi_x - \varphi_\varepsilon) \delta(x - \varepsilon) + \mathcal{P} \left( \frac{\nu(x, \varepsilon)}{x - \varepsilon} \right). \quad (\text{A23})$$

Here,  $\varphi$  is full phase shift (the sum of Coulomb and Hartree–Fock phase shifts) of the electron wave,  $\nu$  is a function expressed through the difference of the corresponding Hartree–Fock potentials, and  $\mathcal{P}$  is the Cauchy principle value of the integral. In the case of  $xl$  and  $\varepsilon l$  states for a single fixed Hartree–Fock potential, we have:

$$\cos(\varphi_x - \varphi_\varepsilon) \rightarrow 1, \quad (\text{A24})$$

$$\mathcal{P} \int_0^\infty \frac{\nu(x, \varepsilon)}{x - \varepsilon} dx \rightarrow 0, \quad (\text{A25})$$

and we return to the integral  $\langle x | \varepsilon \rangle = \delta(x - \varepsilon)$ .

## APPENDIX B

The integration region in (10) is broken up into two subregions:

$$D_1 = \bigcup_{i=1}^m [x_i, x_{i+1}], \quad (\text{B1})$$

$$D_2 = [x_{m+1}, \infty), \quad (\text{B2})$$

where  $x_1 = 0$ ,  $x_{m+1} \cong I_{1s}$ . Over the  $D_1$  region, for every interval  $[x_i, x_{i+1}]$  we take a linear interpolation of the  $\psi$  function,

$$\psi_i = \alpha_i x + \beta_i, \quad (\text{B3})$$

and analytically calculate the Riemann integral:

$$J_1 = \sum_{i=1}^m \int_{x_i}^{x_{i+1}} \psi_i \in_j^{-1} dx. \quad (\text{B4})$$

Over the region  $D_2$ , the following asymptotic form is taken for the square of the radiative transition operator matrix element from Eq. (16):

$$(x + I_{1s})^2 M^2 = \mu_m x^{-1} + \rho_m x^{-2}, \quad (\text{B5})$$

and the improper integral of the first kind is calculated analytically:

$$J_2 = \int_{x_{m+1}}^\infty g_m \in_j^{-1} dx, \quad (\text{B6})$$

$$g_m = \frac{\mu_m x + \rho_m}{(x - \omega + I_{1s})^2 + \gamma_{1s}^2}. \quad (\text{B7})$$

The choice for the asymptotic form (B5) is determined by an analytical estimation of the matrix element in the hydrogen-like approximation for the  $1s$ -electron wave function, and the plane-wave approximation for the wave function of the  $xp$  electron of the continuous spectrum:

$$M \cong x^{-3/2}. \quad (\text{B8})$$

We note that during the calculation of integrals (B4) and (B6) the use of the approximation

$$\gamma_j \rightarrow 0 \Rightarrow L_j \rightarrow \delta(2\omega - \omega_C - I_j - x) \quad (\text{B9})$$

leads to the loss of the Weisskopf–Wigner effect:

$$\gamma = \gamma_{1s} + \gamma_j \rightarrow \gamma_{1s}. \quad (\text{B10})$$

[1] L. Young, K. Ueda, M. Gühr, Ph. H. Bucksbaum, M. Simon, Sh. Mukamel, N. Rohringer, K. C. Prince, C. Masciovecchio, M. Meyer, A. Rudenko, D. Rolles, Ch. Bostedt, M. Fuchs, D. A. Reis, R. Santra, H. Kapteyn, M. Murnane, H. Ibrahim, F. Légaré, M. Vrakking, M. Isinger, D. Kroon, M. Gisselbrecht, A. L'Huillier, H. J. Wörner, and S. R. Leone, *J. Phys. B* **51**,

032003 (2018); Ch. Bostedt, S. Boutet, D. M. Fritz, Zh. Huang, H. J. Lee, H. T. Lemke, A. Robert, W. F. Schlotter, J. J. Turner, and G. J. Williams, *Rev. Mod. Phys.* **88**, 015007 (2016).

[2] T. Åberg and J. Tulkki, in *Atomic Inner-Shell Physics*, edited by B. Crasemann (Plenum Press, New York, 1985), Chap. 10; P. P. Kane, *Phys. Rep.* **218**, 67 (1992).

- [3] F. Gel'mukhanov and H. Ågren, *Phys. Rep.* **312**, 87 (1999); C. Sâthe, F. F. Guimarães, J.-E. Rubensson, J. Nordgren, A. Agui, J. Guo, U. Ekström, P. Norman, F. Gel'mukhanov, and H. Ågren, *Phys. Rev. A* **74**, 062512 (2006); V. Vaz da Cruz, E. Ertan, N. Ignatova, R. C. Couto, S. Polyutov, M. Odelius, V. Kimberg, and F. Gel'mukhanov, *ibid.* **98**, 012507 (2018).
- [4] A. Kotani and S. Shin, *Rev. Mod. Phys.* **73**, 203 (2001); J.-P. Rueff and A. Shukla, *ibid.* **82**, 847 (2010); L. J. P. Ament, M. van Veenendaal, Th. P. Devereaux, J. P. Hill, and J. van den Brink, *ibid.* **83**, 705 (2011).
- [5] K. Tamasaku, E. Shigemasa, Y. Inubushi, T. Katayama, K. Sawada, H. Yumoto, H. Ohashi, H. Mimura, M. Yabashi, K. Yamauchi, and T. Ishikawa, *Nat. Photonics* **8**, 313 (2014).
- [6] S. Ghimire, M. Fuchs, J. Hastings, S. C. Herrmann, Y. Inubushi, J. Pines, S. Shwartz, M. Yabashi, and D. A. Reis, *Phys. Rev. A* **94**, 043418 (2016).
- [7] J. Szlachetko, J. Hozzowska, J.-C. Dousse, M. Nachttegaal, W. Błachucki, Y. Kayser, J. Sá, M. Messerschmidt, S. Boutet, G. J. Williams, Ch. David, G. Smolentsev, J. A. van Bokhoven, B. D. Patterson, Th. J. Penfold, G. Knopp, M. Pajek, R. Abela, and Ch. J. Milne, *Sci. Rep.* **6**, 33292 (2016); K. Tamasaku, E. Shigemasa, Y. Inubushi, I. Inoue, T. Osaka, T. Katayama, M. Yabashi, A. Koide, T. Yokoyama, and T. Ishikawa, *Phys. Rev. Lett.* **121**, 083901 (2018).
- [8] L. M. Kiernan, J. T. Costello, E. T. Kennedy, J.-P. Mosnier, and B. F. Sonntag, *J. Phys. B* **30**, 4801 (1997).
- [9] A. Mihelič, A. Kodre, I. Arčon, J. Padežnik Gomilšek, and M. Borowski, *Nucl. Instrum. Meth. Phys. Res., Sect. B* **196**, 194 (2002).
- [10] L. C. Feldman and J. M. Mayer, *Fundamentals of Surface and Thin Film Analysis* (Elsevier Science Publishing Co., Inc., New York, 1986).
- [11] A. Ecuivillon, G. Israelian, N. C. Santos, M. Mayor, V. Villar, and G. Bihain, *Astron. Astrophys.* **426**, 619 (2004).
- [12] A. I. Akhiezer and V. B. Berestetsky, *Quantum Electrodynamics* (Wiley, New York, 1974).
- [13] A. P. Prudnikov, J. A. Brychkov, and O. I. Marichev, *Integrals and Series* (Gordon and Breach Science, Amsterdam, 1986), Vol. 1.
- [14] Ig. Tamm, *J. Phys. (USSR)* **9**, 449 (1945); V. P. Silin, I. E. Tamm, and V. Ya. Fainberg, *J. Exp. Theor. Phys.* **2**, 3 (1955).
- [15] S. M. Dancoff, *Phys. Rev.* **78**, 382 (1950).
- [16] A. Ganesan, P. C. Deshmukh, and S. T. Manson, *Phys. Rev. A* **95**, 033417 (2017); A. N. Hopersky and A. M. Nadolinsky, *Pis'ma v ZhETF* **108**, 689 (2018) [in Russian].
- [17] A. S. Davydov, *Quantum Mechanics* (Pergamon Press, Oxford, 1976).
- [18] V. Weisskopf and E. Wigner, *Zs. Physik* **63**, 54 (1930); M. A. Blochin, *Physik der Röntgenstrahlen* (VEB Verlag Technik, Berlin, 1965).
- [19] P.-O. Löwdin, *Phys. Rev.* **97**, 1474 (1955); T. Åberg, *ibid.* **156**, 35 (1967); A. P. Jucys, E. P. Našlenas, and P. S. Žvirblis, *Int. J. Quantum Chem.* **6**, 465 (1972); M. Ya. Amusia, *Atomic Photoeffect* (Plenum Press, New York, 1990); A. N. Hopersky and V. A. Yavna, *J. Exp. Theor. Phys.* **82**, 196 (1996); A. Hopersky and A. Nadolinsky, *J. Phys. B* **44**, 075001 (2011).
- [20] M. O. Krause and J. H. Oliver, *J. Phys. Chem. Ref. Data* **8**, 329 (1979).
- [21] Y. Ito, T. Tochio, S. Fukushima, A. Taborda, J. M. Sampaio, J. P. Marques, F. Parente, P. Indelicato, and J. P. Santos, *J. Quant. Spectrosc. Radiat. Transfer* **151**, 295 (2015).
- [22] L. I. Yin, I. Adler, T. Tsang, M. H. Chen, D. A. Ringers, and B. Crasemann, *Phys. Rev. A* **9**, 1070 (1974).
- [23] W. Mehlhorn, B. Breuckmann, and D. Hausamann, *Phys. Scr.* **16**, 177 (1977); M. Y. Adam, S. Stranges, M. de Simone, S. Svensson, and F. Combet Farnoux, *Phys. Rev. A* **49**, 1797 (1994).
- [24] Y. Ito, T. Tochio, M. Yamashita, S. Fukushima, A. M. Vlaicu, Ł. Syrocki, K. Słabkowska, E. Weder, M. Polasik, K. Sawicka, P. Indelicato, J. P. Marques, J. M. Sampaio, M. Guerra, J. P. Santos, and F. Parente, *Phys. Rev. A* **97**, 052505 (2018).
- [25] J. Tulkki and T. Åberg, *J. Phys. B* **15**, L435 (1982).
- [26] M. A. MacDonald, S. H. Southworth, J. C. Levin, A. Henins, R. D. Deslattes, T. LeBrun, Y. Azuma, P. L. Cowan, and B. A. Karlin, *Phys. Rev. A* **51**, 3598 (1995).
- [27] A. Hopersky, A. Nadolinsky, and V. Yavna, *Phys. Rev. A* **75**, 012719 (2007); R. D. Deslattes, R. E. La Villa, P. L. Cowan, and A. Henins, *ibid.* **27**, 923 (1983).
- [28] M. Žitnik, M. Kavčič, K. Bučar, A. Mihelič, M. Štuhec, J. Kokalj, and J. Szlachetko, *Phys. Rev. A* **76**, 032506 (2007); J. Szlachetko, J.-C. Dousse, M. Berset, K. Fennane, M. Szlachetko, J. Hozzowska, R. Barrett, M. Pajek, and A. Kubala-Kukus, *ibid.* **75**, 022512 (2007); D. Sokaras, M. Müller, M. Kolbe, B. Beckhoff, Ch. Zarkadas, and A. G. Karydas, *ibid.* **81**, 012703 (2010).
- [29] A. Hopersky and A. Nadolinsky, *J. Exp. Theor. Phys.* **105**, 549 (2007); H. Czerwinski, F. Smend, D. Schaupp, M. Schumacher, A. H. Millhouse, and H. Schenk-Strauss, *Z. Phys. A* **322**, 183 (1985).
- [30] A. Hopersky, A. Nadolinsky, V. Yavna, and A. Kasprzhitsky, *J. Exp. Theor. Phys.* **104**, 181 (2007).
- [31] D. J. Hudson, *Statistics. Lectures on Elementary Statistics and Probability* (CERN, Geneva, 1964).
- [32] M. Yabashi and H. Tanaka, *Nat. Photonics* **11**, 12 (2017); T. Tanaka, *J. Opt. (Bristol, U. K.)* **19**, 093001 (2017); Ph. Bucksbaum and N. Berrah, *Phys. Today* **68**(7), 26 (2015); J. Feldhaus, M. Krikunova, M. Meyer, Th. Möller, R. Moshhammer, A. Rudenko, Th. Tschentscher, and J. Ullrich, *J. Phys. B* **46**, 164002 (2013).
- [33] A. N. Hopersky, A. M. Nadolinsky, and S. A. Novikov, *J. Phys. B* **50**, 065601 (2017).
- [34] A. N. Hopersky, A. M. Nadolinsky, and R. V. Koneev, *JETP Lett.* **105**, 568 (2017).
- [35] N. Bloembergen, *Nonlinear Optics* (World Scientific, Singapore, 1996).
- [36] A. P. Jucys and A. J. Savukynas, *Mathematical Foundations of the Atomic Theory* (Mintis, Vilnius, 1973) [in Russian].
- [37] R. Karazija, *Introduction to the Theory of X-Ray and Electronic Spectra of Free Atoms* (Plenum Press, New York, 1996).
- [38] G. N. Watson, *A Treatise on the Theory of Bessel Functions* (Cambridge University Press, Cambridge, 1965).
- [39] W. Gordon, *Ann. Phys. (Leipzig)* **2**, 1031 (1929); A. V. Korol, *J. Phys. B* **27**, L103 (1994); S. A. Novikov and A. N. Hopersky, *ibid.* **44**, 235001 (2011); Y. Komninos, T. Mercouris, and C. A. Nicolaides, *Phys. Rev. A* **86**, 023420 (2012); C. Marante, L. Argenti, and F. Martin, *ibid.* **90**, 012506 (2014).